Available online at www.sciencedirect.com
SCIENCE DIRECT®
Polymer 45 (2004) 3913–3922
polymer
www.elsevier.com/locate/polymer

Free volume and transport properties of homogeneous poly(ethylene-*co*-octene)s☆

B. Neway[a], Å. Westberg[a], A. Mattozzi[a], M.S. Hedenqvist[a], M. Giacinti Baschetti[b], V.B.F. Mathot[c], U.W. Gedde[a,*]

[a]*Department of Fibre and Polymer Technology, Royal Institute of Technology, SE-100 44 Stockholm, Sweden*
[b]*Department of Chemical Engineering, Mining and Environmental Technologies, University of Bologna, Viale Risorgimento 2, 40136 Bologna, Italy*
[c]*DSM Research, P.O. Box 18, 6160 MD Geleen, The Netherlands*

Received 17 May 2003; received in revised form 3 December 2003; accepted 3 December 2003

Abstract

Liquid and vapour *n*-hexane sorption/desorption were studied on homogeneous poly(ethylene-*co*-octene)s produced by metallocene-catalyzed polymerisation covering a crystallinity range from 3.5 to 72.4%. Crystal core contents determined by Raman spectroscopy were lower than those determined by density assessments, particularly at low degrees of crystallinity. The solubility showed deviation from Henry's law. The solubilities of *n*-hexane in the homogeneous copolymers depended in a non-linear manner on the content of penetrable polymer component and were lower than those earlier reported for heterogeneous copolymers at the same contents of penetrable component. The concentration dependence of the thermodynamic diffusivity predicted by the Cohen–Turnbull–Fujita free volume theory was confirmed by the data obtained by the differential method and the differences between the results obtained from the integral and differential methods were within the margins of experimental error. The fractional free volume of the penetrable polymer fraction increased with increasing fraction of penetrable polymer and with relative proportion of liquid-like component in the penetrable polymer fraction. The homogeneous copolymers showed a decreasing trend in the geometrical impedance factor with increasing degree of crystallinity.

Keywords: *n*-Hexane diffusion; Poly(ethylene-*co*-octene); Free volume

1. Introduction

The inefficiency of packing of amorphous polymer chains produces an excess free volume in materials [1]. The excess free volume in rubbery polymer phases consists of irregular nanoscopic holes of varying size and it is continuously redistributed as a result of the thermally stimulated motion of the polymer molecules [2]. Small penetrant molecules diffuse across these holes [3]. The pioneering studies by molecular dynamics simulation of Boyd et al. [4–6] presented important molecular details about small-molecule diffusion in amorphous polymer phases. The impermeable crystalline regions force these penetrants to follow a tortuous pathway through the penetrable amorphous regions [7]. The reduction in diffusivity of a semicrystalline polymer with reference to that of a hypothetical wholly amorphous analogue caused by the penetrant detour is commonly expressed as the geometrical impedance factor (τ), the latter being the ratio of the diffusivities in the amorphous and the semicrystalline materials [8]. Boyd [9] derived expressions for upper and lower bound diffusivities in spherulitic polymers. The geometry of a polymer crystal in a melt-crystallized sample is a complex, branched structure that is continuous from the centre to the periphery of the spherulites [10,11]. Previous attempts [12–14] to relate the degree of crystallinity, the crystal shape and the geometrical impedance factor based on the Fricke model [15] and by Monte-Carlo simulation assumed that the impenetrable crystals are lamellar sheets and considered only the lateral crystal dimension as viewed along the crystallographic *b* axis in the analysis. The Fricke model with input data from transmission electron microscopy (lamellar thickness and lateral dimension as

☆ Presented at 'Coupling Simulations and Experiments in Polymer Science: An International Symposium Honoring Professor Richard Boyd', Salt Lake City, Utah, USA, May 15–17, 2003.

* Corresponding author. Tel.: +46-8-790-7640; fax: +46-8-208-856.
E-mail address: gedde@polymer.kth.se (U.W. Gedde).

0032-3861/$ - see front matter © 2004 Elsevier Ltd. All rights reserved.
doi:10.1016/j.polymer.2003.12.083

viewed along *b*), thermal analysis and Raman spectroscopy (crystallinity) predicted the experimentally obtained trend in the geometrical impedance factor for a series of linear polyethylenes [12]. For very high molar mass linear polyethylene, the changes in the geometrical impedance factor were not in quantitative agreement with the Fricke model applied to morphology data [14]. It was argued that the lack of numerical agreement was due to the fact that the assessment of crystal shape by transmission electron microscopy of stained sections systematically underestimated the crystal width, particularly for the low-crystallinity samples with curved and 'twisting' crystal lamellae. A problem was experienced with the heterogeneous branched polyethylenes, which showed a decrease in the geometrical impedance factor with increasing crystallinity [16]. This unusual behaviour was explained by the presence of a few extraordinarily wide crystal lamellae in the heterogeneous low crystallinity samples [16]. The term 'heterogeneous' refers to the uneven distribution of comonomers (short-chain branches) within and between different chains in these particular polymers.

A second influence of the crystals in semicrystalline polymers is the restriction imposed by the crystals on the positional and conformational states of the amorphous chains attached to the crystalline stems [8,12]. Boyd [17] showed that the crystals have a pronounced constraining effect on the amorphous phase resulting in a very high relaxed rubber modulus in polyethylene. Deviation from the liquid-like behaviour of rubbery amorphous component of polyethylene has been demonstrated by proton NMR [18] and Raman spectroscopy [19]. The two effects of the crystals on the diffusivity—the detour and the constraint of the amorphous chains—are conveniently separated by the free volume theory of Cohen and Turnbull [20,21] and Fujita [22] (here denoted the CTF theory):

$$D_T = A \exp(-B_d/f_2) \times \exp((B_d v_1^a (f_1 - f_2))/(f_2(f_2 + v_1^a(f_1 - f_2)))) \quad (1)$$

where D_T is the penetrant thermodynamic diffusivity, A is a factor that is inversely proportional to τ, B_d is a constant that depends only on the size and shape of the penetrant molecule [23], v_1^a is the volume fraction of penetrant in the penetrable phase, f_1 is the fractional free volume of the penetrant and f_2 is the fractional free volume of the penetrable fraction of the polymer. The product of the first two factors in Eq. (1) is equal to the zero-concentration diffusivity. The ability of the penetrant to enhance the diffusivity is quantified by the third factor of Eq. (1). Eq. (1) describes numerically the desorption of *n*-hexane in polyethylene extremely well [12,14,16,23–25]. This is not, however, a proof of its correctness. Neway et al. [14] showed that Eq. (1) gives physically feasible results only for the Doolittle [26], Williams et al. [27] and Cohen and Turnbull [20] free volume scale, i.e. when the fractional free volume at the glass transition temperature is ~0.2–0.3. The fractional free volume (f_1) used for *n*-hexane was, according to Fleischer [25], $f_1 = 0.168$, which yields fractional free volumes for amorphous polyethylene consistent with a fractional free volume of 0.025 at the glass transition temperature.

Previous reports [12,16] on the desorption of *n*-hexane from a collection of different polyethylenes showed that the fractional free volume of the penetrable phase was strongly dependent on its total volume fraction, suggesting the presence of an interfacial penetrable component with a low fractional free volume. The data obtained suggest that mass transport occurs from the liquid-like component to the interfacial component and that the penetrant molecules are trapped at the interfacial sites.

This paper presents data from liquid and vapour *n*-hexane sorption and desorption experiments on a series of metallocene-catalyzed homogeneous poly(ethylene-*co*-octene)s covering a wide range of crystallinity, 3.5 to 72.4% according to density measurements. Solubility data obtained at different penetrant activities for the different polymers provide a direct conversion of 'conventional' diffusivity to thermodynamic diffusivity; the latter being related to the fractional free volume of the penetrable polymer fraction. The study also provides thermodynamic diffusivity data obtained at different penetrant concentrations for the polymers studied, making possible a critical evaluation of the validity of the free volume equation used (Eq. (1)). The correctness of Eq. (1) in describing the penetrant concentration dependence of the thermodynamic diffusivity has been confirmed only for a single linear polyethylene material [28]. Data for the solubility and free volume parameters obtained for the homogeneous poly(ethylene-*co*-octene)s have been compared with previously reported results for Ziegler–Natta-catalyzed heterogeneous poly(ethylene-*co*-octene)s [16].

2. Experimental

The homogeneous poly(ethylene-*co*-octene)s (denoted EOX_{hex}, where X_{hex} is the percentage molar fraction of hexyl branches in the polymer) were synthesized using a Boron-activated metallocene catalyst in a continuously stirred tank reactor. Table 1 presents the molecular characteristics of the polymers studied. The contribution of the polymer chain end groups to X_{hex} is ~0.09 mol%. The polymers were compression-moulded to discs 60 ± 1 mm in diameter and 0.94 ± 0.06 mm thick in a Schwabenthan Polystat 400s compression moulding machine at 433 K for 5 min followed by 0.2 K min^{-1} cooling to 298 K while the pressure was maintained. A second series of samples with a thickness of 50 ± 6 μm were prepared using the same temperature and pressure conditions.

The 0.94 ± 0.06 mm thick polymer discs were immersed in liquid *n*-hexane (purity 99%; Merck; density = 656

Table 1
Molecular structure of polymers studied

Sample code	$\bar{M}_w$ [a] (kg mol^{-1})	$\bar{M}_w/\bar{M}_n$ [a]	Density [b] (kg m^{-3})	MFI_2 [c] (g/10 min)	X_{hex} [d]
EO0.4	73	2.09	955.3	2.39	0.39
EO0.8	–	–	931.7	1.64	0.84
EO1.9	–	–	909.0	1.38	1.92
EO2.3	54	1.93	905.4	10.31	2.33
EO2.4	88	2.44	900.6	1.04	2.36
EO3.6	–	–	882.8	1.23	3.59
EO4.3	–	–	875.9	1.51	4.29
EO5.1	88	2.26	859.3	3.57	5.09

[a] Number average ($\bar{M}_n$) and weight average ($\bar{M}_w$) molar masses by size exclusion chromatography.
[b] At 298 K; standard deviation: ±0.15%.
[c] Melt flow index according to ISO 1133–1991.
[d] Number of hexyl branches per 100 main chain carbon atoms by infrared spectroscopy. The chain ends are included in this figure.

kg m^{-3} at 298 K) at 298 K until sorption equilibrium was reached. The saturated sheets were then kept in air at 298 K and the weights of the discs were intermittently measured using a Mettler AE 100 balance until constant weight was attained. This method is referred to as the integral method. The loss of polymer into *n*-hexane during sorption was low (< 1 wt%) for the majority of the samples. The two samples with the highest degree of branching dissolved to a greater extent: ~3 wt% for sample EO4.3 and more than 50% of sample EO5.1 dissolved during the sorption experiment and was not further studied.

n-Hexane vapour sorption and desorption were also studied at low penetrant activities at 298 K. Films with a thickness of 50 ± 6 μm and weighing 9.5 ± 1 mg were hooked onto the quartz spring and placed in a glass-jacketed column, where the gas pressure could be raised to 101 kPa and measured with an accuracy of 1 Pa. A weight vs. time curve was obtained during the sorption/desorption by recording the sample position in the column using a DVT CCD camera. After evacuating the column, sorption was studied by allowing small amounts of *n*-hexane vapour stepwise into the column, sorption equilibrium being reached for each step. To study the desorption, the penetrant pressure was reduced in steps and the weight loss associated with each step was recorded as a function of time until equilibrium was reached. The recorded kinetics of sorption and desorption, corresponding to the actual penetrant pressure, were used to determine the solubility and the diffusivity of the samples as a function of the partial pressure of penetrant. This method is referred to as the differential method.

Raman spectra were taken for all samples at 298 K using a Perkin–Elmer Spectra 2000 NIR-Raman instrument to determine the mass fractions of the crystal core (CC), interfacial crystal core (ICC), interfacial liquid-like (IL) and liquid-like (L) components of the moulded sheets [19]. These abbreviations are used in the remainder of this paper. For each sample, 150 scans were collected with a resolution of 4 cm^{-1}.

The sample densities were obtained by weighing the moulded sample sheets in air and ethanol (density = 790 kg m^{-3}) and applying the Archimedes principle. These data were converted to mass crystallinity ($w_{c,d}$) considering the densities of the crystalline (1000 kg m^{-3}) and amorphous (855 kg m^{-3}) components reported by Wunderlich [29]. A top-loaded Mettler AE 100 balance with resolution 10^{-5} g and a Mettler-density determination Kit ME-33360 were used.

3. Theory and analysis of sorption and desorption data

The desorption data obtained by the differential method were analysed with Fick's second law for one-dimensional penetrant diffusion assuming constant diffusivity over the limited penetrant concentration range involved in each step [30]:

$$\frac{m_\infty - m_t}{m_\infty} = \frac{8}{\pi^2}\sum_{n=0}^{n=\infty}\frac{1}{(2n+1)^2}\exp\left[-\frac{D(2n+1)^2\pi^2}{4L^2}t\right] \quad (2)$$

where m_t is penetrant mass leaving the polymer sheet after time t, m_∞ is the corresponding quantity after infinite time, D is the diffusivity and L is half the film thickness. D is related to the thermodynamic diffusivity (D_T) according to:

$$D = D_T\left(\frac{\partial(\ln a_1)}{\partial(\ln v_1^a)}\right) \quad (3)$$

where a_1 is the penetrant activity in the polymer. The derivative $(\partial(\ln a_1))/(\partial(\ln v_1^a))$ was obtained from experimental solubility data taken at different penetrant activities.

The following methodology was used in the numerical analysis of the desorption data obtained for samples initially saturated with liquid *n*-hexane ($a_1 = 1$). Further details about the numerical methods used in the integral method have been presented earlier [12,16,31]. The following equation is obtained by insertion of Eq. (3) into the one-dimensional version of Fick's second law of diffusion [31]:

$$\frac{\partial v_1}{\partial t} = \frac{\partial}{\partial x}\left(D_T g\frac{\partial v_1}{\partial x}\right) \quad (4)$$

where D_T is the thermodynamic diffusivity related to v_1^a and f_2 according to Eq. (1), x is the distance from the outer surface of the sheet and $g = (\partial(\ln a_1))/(\partial(\ln v_1^a))$. Only half the sheet thickness was considered in the numerical solution. The following inner and outer boundary conditions

were applied in the numerical analysis of Eq. (4):

$$\left(\frac{\partial v_1}{\partial x}\right)_{x=L} = 0 \tag{5}$$

$$D_T g(v_1^a)\left(\frac{\partial v_1}{\partial x}\right)_{x=0} = F_0(v_1)_{x=0} \tag{6}$$

where F_0 is the rate of evaporation from the surface of the sheet during desorption and was calculated from the initial rate of desorption [32]:

$$F_0 = \frac{\mathrm{d}m_t/\mathrm{d}t}{2S(C_0 - C_{eq})} \tag{7}$$

where S is the area of the sample surface, C_0 is the penetrant concentration in the immediate sample surface during the initial stage of desorption and $C_{eq} = 0$ is the equilibrium penetrant concentration with the *n*-hexane-free surroundings.

The parameters A and f_2 were adjustable in the fitting of Eqs. (1) and (4–7) to the experimental data. The constants $f_1 = 0.168$ and $B_d = 0.8$ in Eq. (1), were taken from Fleischer [25]. Two different assumed systems of penetrable phases were analyzed; In method 1; L, IL and ICC components were assumed to be penetrable. In method 2; L and IL components were assumed to be penetrable phases. The mass fractions of the components (w_i) shown in Table 2 were converted into volume fraction (v_i) from ρ_2 according to:

$$v_i = \frac{w_i \rho_2}{\rho_i} \qquad i = \mathrm{CC,\ L\ or\ ICC} \tag{8}$$

where ρ_2 and ρ_i are, respectively, the densities of the polymer and of its components. The following density values were used: $\rho_{CC} = 1000\ \mathrm{kg\ m^{-3}}$ [29], $\rho_L = 855\ \mathrm{kg\ m^{-3}}$ [29] and $\rho_{ICC} = 930\ \mathrm{kg\ m^{-3}}$ [12,16].

Table 2
Mass crystallinities and mass fractions of components by Raman spectroscopy at 298 K

Sample code	$w_{c,d}$ [a]	w_{CC} [b,c]	w_{ICC} [b]	w_{IL} [b,d]	w_L [b,e]
EO0.4	0.724	0.715	0.071 ± 0.034	0.052	0.162
EO0.8	0.568	0.552	0.099 ± 0.027	0.092	0.257
EO1.9	0.410	0.340	0.135 ± 0.021	0.111	0.414
EO2.3	0.384	0.274	0.143 ± 0.020	0.130	0.453
EO2.4	0.349	0.244	0.150 ± 0.020	0.113	0.493
EO3.6	0.217	0.056	0.136 ± 0.023	0.136	0.672
EO4.3	0.165	0.018	0.149 ± 0.024	0.128	0.705
EO5.1	0.035	0	–	–	–

[a] Mass crystallinity ($w_{c,d}$) from density data; relative error ± 6%.
[b] Mass fractions of crystal core (w_{CC}), interfacial crystal core (w_{ICC}), interfacial liquid-like (w_{IL}) and liquid like (w_L) components by Raman spectroscopy according to Refs. [16,19].
[c] Relative error ±5%.
[d] Relative error ±4%.
[e] Relative error ±3%.

4. Results and discussion

4.1. Crystallinity and phase composition

Fig. 1 shows the crystallinity assessed by density measurements and Raman spectroscopy as a function of hexyl-branch content. The polymers studied covered a broad range of crystallinity from 3.5 to 72.4%. The sample with 5 mol% hexyl branches showed no crystal core component according to Raman spectroscopy. The density-based crystallinity ($w_{c,d}$) approached zero at ~6 mol% hexyl branches, which is in the same range as that found for heterogeneous poly(ethylene-*co*-octene)s [16]. The CC content was similar to the density-based crystallinity for the highly crystalline samples, $w_{c,d} > 0.55$, whereas the low crystalline samples showed a density-based crystallinity larger than the CC content; the difference between the two increased with decreasing crystallinity (Fig. 1). This is exactly the same trend that was found by Neway et al. [16] for the heterogeneous poly(ethylene-*co*-octene)s. They reported that the average difference $w_{c,d} - w_{CC}$ was 0.085 for heterogeneous poly(ethylene-*co*-octene)s, which was on an average 22% of the crystalline content as assessed by density measurements. The corresponding values for the homogeneous copolymers, considering samples within the same range of comonomer content as the heterogeneous poly(ethylene-*co*-octene)s were 0.079 and 25%. Lagarón et al. [33] found that the CC content assessed by Raman spectroscopy was lower than the crystallinity determined by DSC or WAXS and that the difference between the two crystallinities increased with decreasing density. They suggested that small defective crystals with a lateral disorder were present in low crystallinity samples and that these are not included for in the CC component by Raman spectroscopy.

Table 2 presents the mass crystallinities obtained from density measurements and the mass fractions of the components assessed by Raman spectroscopy. The proportion of

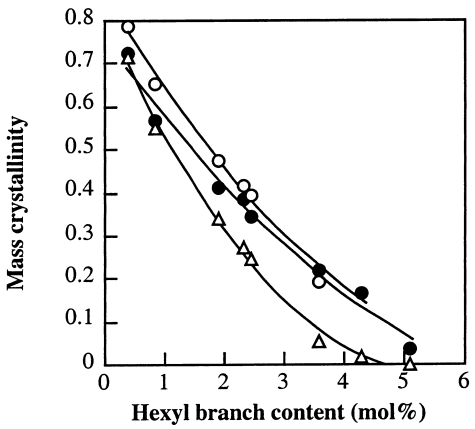

Fig. 1. Mass crystallinity as a function of hexyl branch content: (●) from density data, $w_{c,d}$; (△) from Raman spectroscopy, w_{CC}; (○) from Raman spectroscopy, $w_{CC} + w_{ICC}$.

the L component in the penetrable phases, ICC + IL + L or IL + L depending on the method used, increased with decreasing density: $(w_L)/(w_{ICC} + w_{IL} + w_L)$ ranged from 0.567 (sample EO0.4) to 0.719 (sample EO4.3) and $w_L/(w_{IL} + w_L)$ ranged from 0.756 (sample EO0.4) to 0.847 (sample EO4.3). These data are consonant with the trend previously reported for high molar mass polyethylene [14] and heterogeneous poly(ethylene-*co*-octene)s [16].

Fig. 2 shows the CH_2 bending (1390–1510 cm^{-1}) region of the Raman spectrum of samples EO0.4 and EO5.1. The 1417 cm^{-1} peak associated with the CC component [19] was not present in the spectrum of EO5.1. Moreover, the spectrum of EO5.1, unlike those of the other samples, could not be described by the sum of three Lorenz equations. Sample EO5.1 with only 3.5% mass crystallinity according to density measurements contained only small defective crystals that were not revealed by Raman spectroscopy as CC component.

4.2. Solubility as a function of partial pressure of penetrant

Fig. 3 presents the solubility of the penetrant in one of the polymers studied as a function of the penetrant activity, $a_1 = p/p^s$ (where p is the partial pressure of *n*-hexane and p^s is the saturated vapour pressure of *n*-hexane). The solubilities were obtained during sorption. The other polymers studied showed similar solubility vs. a_1 curves. A pronounced deviation from the Henry law behaviour (i.e. a straight line) is evident. The insert in Fig. 3 shows the log–log diagram from which the thermodynamic correction factor was obtained (Eq. (3)).

A second order polynomial was fitted to the experimental data shown in the insert graph of Fig. 3. The first derivative of the fitted polynomial was represented as follows:

$$\frac{\partial(\ln a_1)}{\partial(\ln v_1^a)} = \left\{ \begin{array}{ll} 2\alpha \ln v_1^a + \beta & \text{for } v_1^a \geq 0.005 \\ 1 & \text{for } v_1^a < 0.005 \end{array} \right\} = g \qquad (9)$$

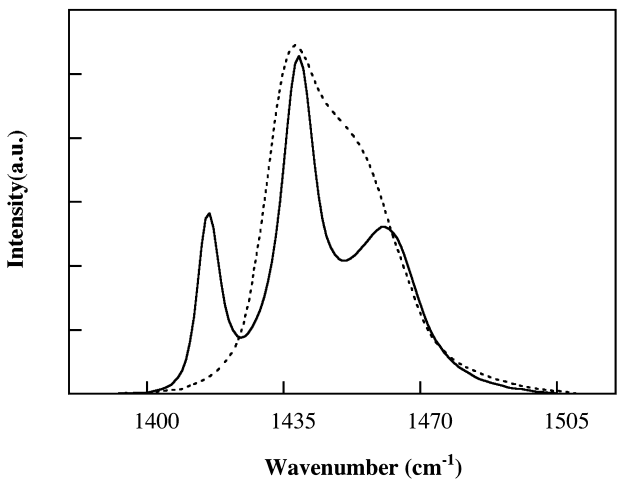

Fig. 2. Raman spectra of CH_2 bending region: continuous line for sample EO0.4 and broken line for sample EO5.1.

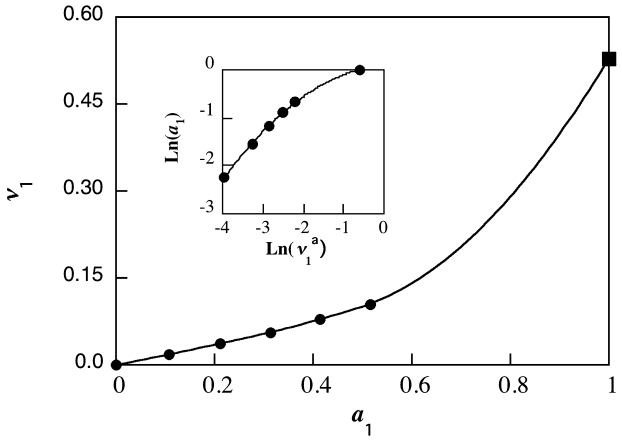

Fig. 3. Equilibrium volume fraction of *n*-hexane in sample EO3.6 as a function of *n*-hexane activity. The data point marked with (■) refers to the sample exposed to liquid *n*-hexane. The insert diagram shows the dependence of $\ln a_1$ on $\ln v_1^a$. The continuous line in the insert figure represents the second order polynomial fit.

where α and β are constants for a given polymer (Table 3). To avoid the singularity at $v_1^a = 0$, the thermodynamic correction term was set to 1 at a very low solubility, 0.005. It was found that the value used to avoid the singularity had only a negligible effect on the fitted values for the adjustable parameters A and f_2. The data obtained for sample EO0.4 was too noisy to permit an accurate determination of α and β.

4.3. Penetrant solubility of polymer in liquid n-hexane ($a_1 = 1$)

Fig. 4 presents the solubility of liquid *n*-hexane as a function of penetrable polymer fraction (v_{pen}), i.e. contents of L, IL and ICC (method 1) and of I and IL (method 2), for both the homogeneous copolymers studied and the heterogeneous copolymers reported earlier [16]. The solubility increased in an accelerating fashion with increasing v_{pen}, i.e. the solubility of penetrant in the penetrable fraction increased with increasing v_{pen}. This resembled the behaviour of thermoplastic elastomers with the crystals acting as physical crosslinks and the amorphous chain segments deforming as a consequence of the swelling. The high penetrant solubility in samples with low crystallinity is thus due to their long amorphous chain segments. The penetrant

Table 3
Thermodynamic correction factor parameters (Eq. (9))

Sample	Method 1		Method 2	
	α	β	α	β
E00.8	0.0048	0.9574	0.0069	0.9829
EO1.9	−0.0501	0.5548	−0.0446	0.6176
EO2.3	−0.0784	0.3341	−0.0749	0.3948
EO2.4	−0.0708	0.3906	−0.0669	0.4510
EO3.6	−0.1361	0.0517	−0.1356	0.0981
EO4.3	−0.1725	0.0332	−0.1751	0.0815

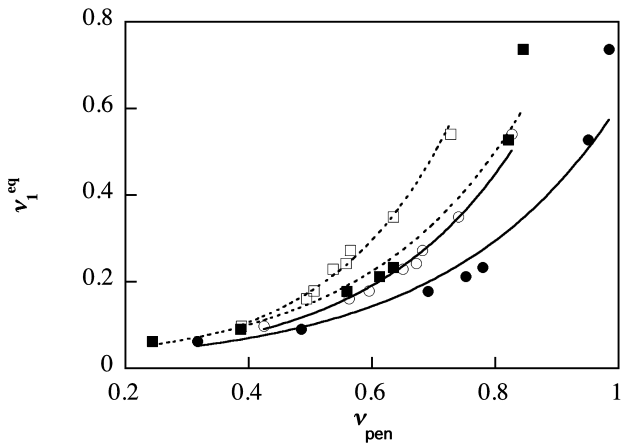

Fig. 4. Equilibrium volume fraction of *n*-hexane in polymer (v_1^{eq}) as a function of the volume fraction of penetrable components in dry polymer (v_{pen}). Method 1 (I, IL and ICC were penetrable): (●) homogeneous poly(ethylene-*co*-octene)s; (○) heterogeneous poly(ethylene-*co*-octene)s, data from Neway et al. [16]. Method 2 (I and IL were penetrable): (■) homogeneous poly(ethylene-*co*-octene)s; (□) heterogeneous poly(ethylene-*co*-octene)s, data from Neway et al. [16].

solubility of a series of heterogeneous copolymers was calculated from the Flory–Rehner equation [34] but, although the calculation showed the correct trends in the experimental data, they were not capable of accurate prediction. The inadequacy of the simple Flory–Rehner equation applied to the present case has several causes: (i) cilia do not contribute to the elastic swelling forces; (ii) the amorphous chain segments can be very short, particularly in the highly crystalline systems, and swelling may deform the amorphous segments beyond the limit of the Gaussian approximation; (iii) the crystal lamellae will act as a constraint on swelling in the lamellar plane. The data presented in Fig. 4 will be subjected to a careful theoretical analysis including these missing features in a coming study.

Fig. 4 shows that the solubility was lower in the homogeneous copolymers than in the heterogeneous analogues. The difference was particularly pronounced for the samples with high v_{pen} values. The heterogeneous copolymers possessed an extremely broad melting temperature range, essentially from 290 to 400 K [16]. The morphological heterogeneity permits very extensive swelling of the regions with low crystallinity and low melting point. It thus seems that the penetrant uptake in these 'loose' regions dominated over the reduction in swelling of the regions with high crystallinity and high melting point.

4.4. Desorption from the saturated state at $a_1 = 1$; fitting of the free volume equation

Table 4 presents data obtained for the adjustable parameters (A and f_2), the zero-concentration diffusivity ($D_{v_1 \to 0}$) and the sum-of-squares-difference (SSD) between normalized fitted and experimental data for the two methods employed. The error estimation for the adjustable parameter A gave results with an average deviation of ±9 and ±5% from the final optimum values for methods I and II, respectively. Values of f_2 were within ±1% of the optimum values reported. Values of $D_{v_1 \to 0}$ were estimated with an average of ±5 and ±4% deviation from the optimum values for methods I and II, respectively. The error estimation was based on a sensitivity analysis, which considered the experimental error involved in the determination of the fraction of penetrable components. For method 1, a 5% relative error of CC component was considered in the error analysis (note: $1 - w_{CC} = w_{ICC} + w_{IL} + w_L$). For method 2, a 2.5% uncertainty of the penetrable components (IL + L) was used in the error analysis. The excellent fit of the desorption data for sample EO1.9 is shown in Fig. 5. As the SSD data show in Table 4, the goodness of the fit was similar for both methods, and in both cases the goodness of fit was very high, except for sample EO4.3 analysed by method 2.

Fig. 6a and b show that the fractional free volume of the penetrable polymer (f_2) was proportional to the volume fraction of the penetrable component. The data for the homogeneous copolymers are shown together with earlier data reported by Neway et al. [16] for heterogeneous poly(ethylene-*co*-octene)s. The agreement between the data for homogeneous and heterogeneous copolymers was good in the case of method 1 (Fig. 6a). The data obtained by method 2 yielded higher f_2 values for the homogeneous copolymers than for the heterogeneous copolymers, particularly for the highly crystalline samples (Fig. 6b).

The f_2 obtained by method 2, excluding sample EO4.3 was on average 0.0030 higher than the value obtained by method 1. The corresponding value for the heterogeneous copolymers was 0.0007 [16]. It should be noted that different methods were used to determine the thermodynamic correction factor defined in Eq. (3) for the two series of samples. For the heterogeneous copolymers, the

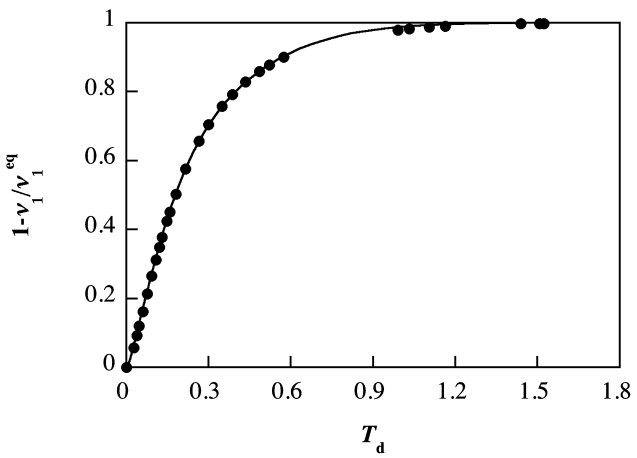

Fig. 5. Normalized *n*-hexane desorption curves for sample EO1.9 showing experimental data (points) and fitted data (line) according to method 1. Dimensionless time (T_d) is defined as $T_d = \sqrt{D_{v_1 \to 0} t / L^2}$, where $D_{v_1 \to 0}$ is the diffusivity at $v_1 = 0$, t is time and L is half the specimen thickness. The *n*-hexane concentration (v_1) is normalized with respect to the equilibrium penetrant concentration (v_1^{eq}) at $a_1 = 1$.

Table 4
Free volume parameters obtained by fitting according to methods 1 and 2

Sample	Method 1				Method 2			
	f_2[a]	A[b,c]	$D_{v_1\to 0}$[d,e]	SSD[f]	f_2[a]	A[c,d]	$D_{v_1\to 0}$[e,g]	SSD[f]
EO0.4	0.0436	0.0818	0.0988	0.0033	0.0464	0.0241	0.0784	0.0043
EO0.8	0.0469	0.0646	0.252	0.0042	0.0504	0.0185	0.235	0.0044
EO1.9	0.0598	0.0178	2.75	0.0004	0.0628	0.0084	2.47	0.0005
EO2.3	0.0624	0.0155	4.19	0.0058	0.0671	0.0064	4.25	0.0052
EO2.4	0.0643	0.0135	5.33	0.0019	0.0664	0.0076	4.45	0.0008
EO3.6	0.0723	0.0075	11.8	0.0039	0.0739	0.0053	10.5	0.0036
EO4.3	0.0784	0.0061	22.5	0.0087	0.0749	0.0062	14.3	0.0101

[a] Relative error ± 1%.
[b] Relative error ± 9%.
[c] In $cm^2\ s^{-1}$.
[d] Relative error ± 5%.
[e] Diffusivity at $v_1 = 0$ in $10^{-8}\ cm^2\ s^{-1}$.
[f] SSD, sum-of-squares-difference between normalised experimental and fitted desorption data.
[g] Relative error ± 4%.

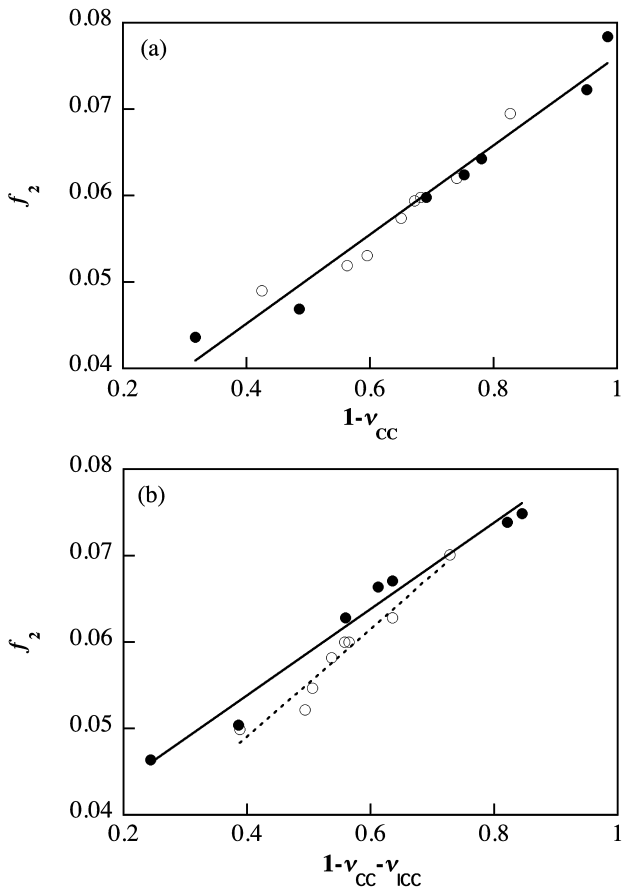

Fig. 6. The fractional free volume of penetrable polymer (f_2) as a function of the volume fraction of penetrable polymer for homogeneous poly(ethylene-*co*-octene)s (●) and heterogeneous poly(ethylene-*co*-octene)s according to Neway et al. [16] (○). The straight lines represent linear fits to the experimental data: (a) method 1; (b) method 2.

Flory–Huggins theory was used and literature data for the interaction parameter was used in the calculation of the correction factor. For the homogeneous copolymers the thermodynamic correction term was determined from sorption equilibria at different *n*-hexane activities as shown in Fig. 3 with one exception: sample EO0.4.

In a previous paper [16], three different diffusion models were tested on the free volume (f_2) data obtained for the heterogeneous copolymer samples. The models were: (i) the 'solution model': the liquid-like and interfacial components were uniformly mixed and the effective free volume of the solution is represented by $f_2 = f_2^{\mathrm{I}} + v_{\mathrm{L}}^n(f_2^{\mathrm{L}} - f_2^{\mathrm{I}})$; (ii) the 'series model': the liquid-like and interfacial components were connected in series in the diffusion system between the two crystal lamellae; (iii) the 'parallel model': the liquid-like and interfacial components were connected in parallel in the diffusion system located between the two crystal lamellae. No mass transport was allowed between two components. Further details of the models can be found in Ref. [16]. None of the three models was, however, capable of describing the experimental data obtained for the heterogeneous copolymers [16]. The same was true for the homogeneous copolymers. The inadequacy of the models in describing the experimental data obtained for both homogeneous and heterogeneous copolymers is shown in Figs. 7 and 8. Linear extrapolation of the data presented in Fig. 7 to $v_{\mathrm{L}}^n = 0$ yields negative values for f_2^{I}; method 2 (not shown in Fig. 7) also yielded negative values for f_2^{I}. Another negative feature of the appearance of the solution model is the fact that the data for the homogeneous and heterogeneous copolymers adapt to different lines (Fig. 7). The series and parallel models are both inadequate, as is clearly shown in Fig. 8.

Neway et al. [16] proposed, on the basis of these 'failures', an alternative model assuming mass transport between the liquid-like and interfacial components arranged in a parallel fashion in the crystal–amorphous–crystal

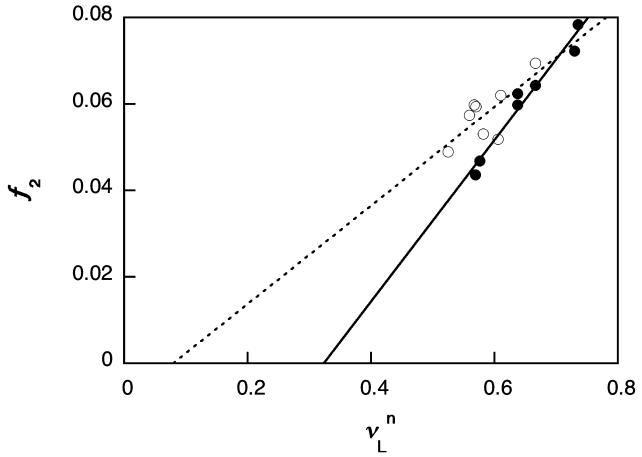

Fig. 7. The fractional free volume of penetrable polymer (f_2) as a function of the volume fraction of liquid-like component in the penetrable fraction of the polymer (v_L^n) for homogeneous poly(ethylene-*co*-octene)s (●) and heterogeneous poly(ethylene-*co*-octene)s according to Neway et al. [16] (○). The straight lines represent linear fits to the experimental data. The presented data were obtained by method 1.

sandwich. It is here suggested that the pronounced depression in diffusivity, i.e. the decrease in effective free volume of the penetrable component characteristic of the semicrystalline systems is due to trapping of the penetrant molecules at interfacial sites.

The data obtained for the pre-exponential factor (A), which is inversely proportional to the geometrical impedance factor (τ), are presented both in Table 4 and in a graphical form as a function volume fraction of penetrable polymer phase in Fig. 9a and b. The data show that A increases with increasing crystallinity. This surprising behaviour was previously reported for the heterogeneous poly(ethylene-*co*-octene)s [16]. The general decreasing trend in the A-penetrable volume fraction data was the

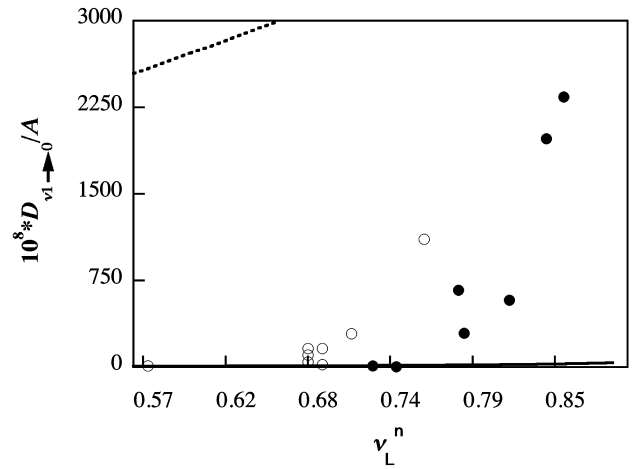

Fig. 8. Amorphous zero-concentration diffusivity divided by A as a function of volume fraction of liquid-like component in the penetrable fraction of the polymer (v_L^n) for homogeneous poly(ethylene-*co*-octene)s (●) and heterogeneous poly(ethylene-*co*-octene)s according to Neway et al. [16] (○). The broken and the continuous lines represent the results from parallel and series diffusion models, respectively.

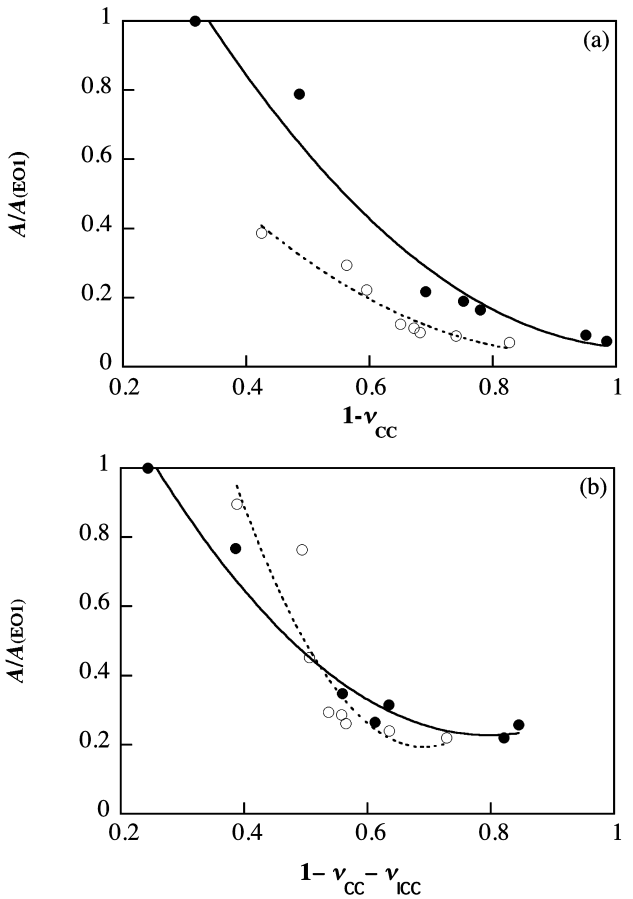

Fig. 9. Normalized pre-exponential factor A as a function of the volume fraction of penetrable polymer for homogeneous poly(ethylene-*co*-octene)s (●) and heterogeneous poly(ethylene-*co*-octene)s according to Neway et al. [16] (○): (a) method 1; (b) method 2.

same for both the homogeneous and heterogeneous copolymers. According to method 1, A is larger (i.e. the geometrical impedance factor is smaller) for the homogeneous copolymers than for the heterogeneous analogues (Fig. 9a). Method 2 yielded data for both types of copolymers falling on a single curve (Fig. 9b). The increase in A with increasing crystallinity was explained by the importance of the effect of the crystal morphology on the diffusion of the penetrant, i.e. the presence of extraordinarily wide crystal lamellae in the low crystallinity samples [35]. Morphological characterization assessing the shape of the crystals of the different homogeneous copolymers will be reported in a coming paper.

4.5. Diffusivity obtained by the differential method at low n-hexane activity

Table 5 present the zero-concentration diffusivities obtained by the integral and differential methods. The differential data were only analyzed according to method 1 (I, IL and ICC are penetrable components). The diffusivities obtained by the: differential method were on an average 40% smaller than those obtained by the integral method.

Table 5
Zero-concentration diffusivities and parameters of the free volume equation at 298 K obtained by different methods

Sample code	$D_{v_1\to 0}$ [a,b]	f_2; A [c]	$D_{v_1\to 0}$ [a,d]	f_2; A [e]
EO0.8	0.252	0.0464; 0.0646	0.045	0.0394; 0.297
EO1.9	2.75	0.0598; 0.0178	1.68	0.0584; 0.0149
EO2.3	4.19	0.0624; 0.0155	3.05	0.0615; 0.0136
EO2.4	5.33	0.0643; 0.0135	3.66	0.0600; 0.0260
EO3.6	11.8	0.0723; 0.0075	8.50	0.0807; 0.0017
EO4.3	22.5	0.0784; 0.0061	12.0	0.0880; 0.0011

[a] Diffusivity at $v_1 = 0$ in 10^{-8} cm^2 s^{-1}.
[b] By integral method 1, relative error ± 5%.
[c] Free volume equation parameter values by integral method 1; A is given in cm^2 s^{-1}.
[d] By differential method 1, with thermodynamic correction.
[e] Free volume equation parameter values by differential method 1; A is given in cm^2 s^{-1}.

These differences are within the margins of experimental error. Furthermore, the samples were exposed to the penetrant for different periods of time and also the 'prehistorical' penetrant concentration was different for the integral and the differential methods. It is known from earlier studies [31] that this has an effect on the diffusivity.

Fig. 10 shows the diffusivity obtained from integral desorption data for method 1 and the diffusivity obtained from the differential desorption kinetics for sample EO1.9. The diffusivity obtained from the integral desorption kinetics was higher in this particular case than that obtained from the differential desorption kinetics over the whole investigated concentration range. The curved trend with a negative second derivative characteristic of the integral method based on free volume theory is also apparent in the data obtained by the differential method. Hence, these data support the free volume model used in the calculations (integral method) and shows that this method is preferred over to the empirical exponential law: $D = D_{v_1\to 0}\exp(\gamma v_1)$, where γ is a constant for a given penetrant–polymer pair.

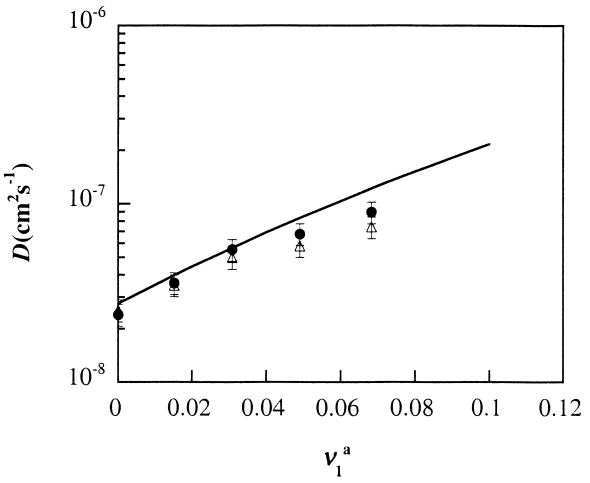

Fig. 10. n-Hexane diffusivity in sample EO1.9 as a function of the volume fraction of n-hexane: The continuous line represents the results from the integral desorption measurements using free volume theory (method 1) and (△) thermodynamic diffusivity from measurements at low n-hexane activity (differential method 1).

The parameters of the free volume equation, f_2 and A, showed the same trends with respect to the degree of crystallinity for both methods used (Table 5). The fractional free volume obtained by the two methods were on an average the same; the difference between the two sets of f_2 data was less than 1% (relative value). The geometrical factor A obtained by the differential methods decreased more strongly with decreasing crystallinity than that obtained by the integral method (Table 5).

5. Conclusions

The proportion of defective crystals present in the homogeneous poly(ethylene-*co*-octene)s increased with decreasing degree of crystallinity. The solubility of n-hexane in the polymers as a function of penetrant activity (a_1) deviated markedly from Henry's law. The solubility of n-hexane at $a_1 = 1$ in the penetrable polymer fraction increased with increasing volume fraction of penetrable polymer resembling the behaviour of thermoplastic elastomers. The solubility of n-hexane was lower in the homogeneous copolymers than in the analogues heterogeneous copolymers earlier reported [16]. The morphological heterogeneity of the heterogeneous copolymers permits extensive swelling of regions of low crystallinity and low melting point. The concentration dependence of the thermodynamic diffusivity predicted by the Cohen–Turnbull–Fujita free volume theory was confirmed by the data obtained by the differential desorption measurements. The fractional free volume of the penetrable polymer fraction (f_2) increased with increasing volume fraction of penetrable component. It is suggested that the increase in f_2 with increasing fraction of penetrable polymer and with the relative proportion of liquid-like component in the penetrable polymer fraction is due to trapping of penetrant molecules at interfacial sites. The homogeneous copolymers showed like the heterogeneous a decreasing trend in the geometrical impedance factor with increasing degree of crystallinity. The two different methods used in the analysis—method 1 (interfacial crystal core, interfacial liquid-like and liquid-like components are penetrable) and method 2 (interfacial liquid-like and liquid-like components are penetrable)—gave numerically similar results in terms of goodness of fit. Method 1 yielded results for f_2 that were almost identical for both heterogeneous and homogeneous copolymers and different results for A (parameter relating to the geometrical impedance factor) for the two series of polymers. This trend seems physically more realistic than the results obtained by method 2; the latter showed different results for f_2 and almost the same for A for the heterogeneous and homogeneous copolymers.

Acknowledgements

This work was sponsored by the Swedish Agency for Research Co-operation with Developing Countries (SAREC/SIDA) through the joint collaboration of the University of Asmara, Eritrea and the International Science Programs (ISP) of Uppsala University, Sweden.

References

[1] Simha R, Carri G. J Polym Sci, Polym Phys 1994;32:2645.
[2] Ghosal K, Freeman BD. Polym Adv Technol 1994;5:673.
[3] Jordan SS, Koros WJ. Macromolecules 1995;28:2228.
[4] Pant PVK, Boyd RH. Macromolecules 1992;25:494.
[5] Pant PVK, Boyd RH. Macromolecules 1992;26:679.
[6] Han J, Boyd RH. Polymer 1996;37:1797.
[7] Peterlin A. J Macromol Sci Phys B 1975;11:57.
[8] Michaels A, Bixler HJ. J Polym Sci 1961;50:413.
[9] Boyd RH. J Polym Sci, Polym Phys 1983;21:505.
[10] Basssett DC, Hodge AM. Proc R Soc London 1978;A359:121.
[11] Gedde UW, Mattozzi A. Adv Polym Sci 2004; in press.
[12] Hedenqvist M, Angelstok AA, Edsberg L, Larsson PT, Gedde UW. Polymer 1996;37:2887.
[13] Hadgett PM, Goldbeck-Wood G, Windle AH. Polymer 2000;41:6151.
[14] Neway B, Hedenqvist MS, Gedde UW. Polymer 2003;44:4003.
[15] Fricke H. Phys Rev 1924;24:575.
[16] Neway B, Hedenqvist MS, Mathot VBF, Gedde UW. Polymer 2001; 42:5307.
[17] Boyd RH. Polym Engng Sci 1979;(19):1010.
[18] Kitamaru R, Horii F, Hyon S-H. J Polym Sci, Polym Phys 1977;15: 821.
[19] Mutter R, Stille W, Strobl G. J Polym Sci, Polym Phys 1993;31:99.
[20] Cohen MH, Turnbull D. J Chem Phys 1959;31:1164.
[21] Turnbull D, Cohen MH. J Chem Phys 1970;52:3038.
[22] Fujita H. Fortschr Hochpolym Forsch 1961;3:1.
[23] Kulkarni SS, Stern SA. J Polym Sci, Polym Phys 1983;21:441.
[24] Fels M, Huang RYM. J Appl Polym Sci 1970;14:523.
[25] Fleischer G. Colloid Polym Sci 1984;262:919.
[26] Doolittle AK. J Appl Phys 1951;22:1471.
[27] Williams ML, Landel RF, Ferry JD. J Am Chem Soc 1955;77:3701.
[28] Hedenqvist MS, Doghieri F. Polymer 2002;43:223.
[29] Wunderlich B, Macromolecules physics: crystal structure, morphology and defects, vol. 1. New York: Academic Press; 1973.
[30] Crank J. The mathematics of diffusion, 2nd ed. Oxford: Oxford University Press; 1975.
[31] Hedenqvist MS, Gedde UW. Polymer 1999;40:2381.
[32] Bakhouya A, Brouzi AE, Bouzon J, Vergnaud JM. Plast Rubber Compos Process Appl 1993;19:77.
[33] Lagarón J, López-Quintana S, Rodriguez-Cabello J, Merino J, Pastor J. Polymer 2000;41:2999.
[34] Flory PJ, Rehner J. J Chem Phys 1943;11:521.
[35] Deblieck RAC, Mathot VBF. J Mater Sci Lett 1988;7:1276.